Geophysical Research Letters

RESEARCH LETTER
10.1029/2019GL084589

Subsurface Water Dominates Sierra Nevada Seasonal Hydrologic Storage

Thomas L. Enzminger[1], Eric E. Small[1], and Adrian A. Borsa[2]

[1]Department of Geological Sciences, University of Colorado Boulder, Boulder, CO, USA, [2]Scripps Institution of Oceanography, University of California, San Diego, La Jolla, CA, USA

Key Points:
- Seasonal subsurface water storage (soil moisture and groundwater) in the Sierra Nevada dominates local solid Earth elastic deformation
- Water in snow accounts for about 30% of total storage but varies from ~25–50% depending on the time of year
- Seasonal maxima in total water storage exceed accumulated precipitation totals, suggesting that precipitation is underestimated

Supporting Information:
- Supporting Information S1
- Table S1

Correspondence to:
T. L. Enzminger,
thomas.enzminger@colorado.edu

Citation:
Enzminger, T. L., Small, E. E., & Borsa, A. A. (2019). Subsurface water dominates Sierra Nevada seasonal hydrologic storage. *Geophysical Research Letters*, *46*, 11,993–12,001. https://doi.org/10.1029/2019GL084589

Received 16 JUL 2019
Accepted 2 OCT 2019
Accepted article online 16 OCT 2019
Published online 5 NOV 2019

Abstract Vertical displacements (dz) in permanent Global Positioning System (GPS) station positions enable estimation of water storage changes (ΔS), which historically have been impossible to measure directly. We use dz from 924 GPS stations in the western United States to estimate daily ΔS in California's Sierra Nevada and compare it to seasonal snow accumulation and melt over water years 2008–2017. Seasonal variations in GPS-based ΔS are ~1,000 mm. Typically, only ~30% of ΔS is attributable to snow water equivalent (SWE). ΔS lags the snow cycle, peaking after maximum SWE and remaining positive when all snow has melted (SWE = 0). We conclude that seasonal ΔS fluctuations are not primarily driven by SWE but by rainfall and snowmelt stored in the shallow subsurface (as soil moisture and/or groundwater) and released predominantly through evapotranspiration. Seasonal peak GPS ΔS is larger than accumulated precipitation from the Parameter-elevation Relationships on Independent Slopes Model and North American Land Data Assimilation System, indicating that these standard inputs underestimate mountain precipitation.

Plain Language Summary When a large amount of water is added to an area of the Earth's surface—such as through a storm in the mountains—its weight compresses the solid Earth, causing the land surface to move downward. When the water evaporates or runs off, the land surface rebounds instantly. In the western United States, a network of permanent Global Positioning System (GPS) stations measures these vertical motions of the land surface at high precision. We use GPS data to estimate the amount and distribution of changes in water mass in the Sierra Nevada of California. Water stored underground (as soil moisture and groundwater) is very difficult to measure compared to snow, which can be estimated reasonably accurately with satellite remote sensing. Using GPS data, we calculate the amount of underground storage: the total mass minus independent estimates of the mass of snow. We find that underground storage makes up the majority (70%) of total stored water. Furthermore, the amount of water estimated by GPS is larger than independent estimates of total precipitation (rain + snow). This suggests that more precipitation falls in the Sierra Nevada than has previously been thought, and this precipitation is mainly stored underground.

1. Introduction

Seasonal water storage in California's Sierra Nevada (SN) plays a vital role in the state's annual water budget. Streamflow, fed by mountain precipitation that accumulates during the winter wet season (November–April), is crucial to sustaining downstream urban populations, agriculture, and ecosystems over hot, dry summers. Snowpack storage is estimated to supply 50–80% of regional streamflow (e.g., Doesken and Judson (1996); Li et al. (2017)). However, precipitation stored as soil moisture and groundwater is the moisture source for SN evapotranspiration and ecosystem productivity (Henn, Painter, et al., 2018). Thus, the partitioning of stored precipitation into streamflow versus evapotranspiration is a critical hydrologic process. This partitioning is expected to be sensitive to climate change (Berghuijs et al., 2014).

At the mountain range scale, changes in water storage (ΔS) can be represented by the simple water balance

$$\Delta S = P - ET - Q \quad (1)$$

where P is precipitation, ET is evapotranspiration, and Q is streamflow. ΔS generally increases throughout the wet season—when the SN receives ~90% of its annual precipitation—and decreases during the dry season (approximately May–October). Streamflow and evapotranspiration remove stored water throughout the water year (WY) but particularly in spring and summer when rates are highest. Rain-snow precipitation

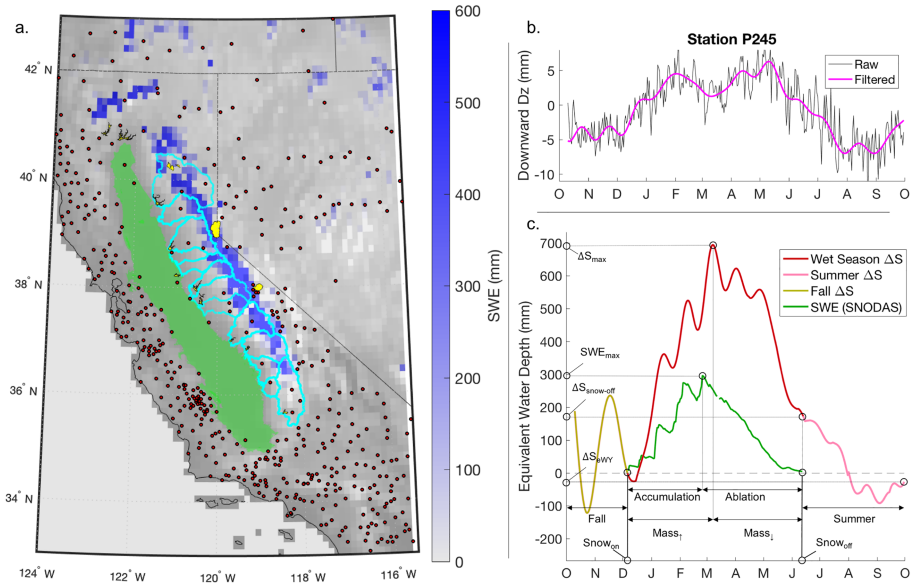

Figure 1. (a) Overview of the Sierra Nevada, including distribution of SNODAS SWE (blue) for 1 April 2008, Sierra Nevada basin boundaries (cyan) and locations of GPS stations (red circles), large lakes/reservoirs (yellow), and the Central Valley (green). (b) Example seasonal GPS dz time series (raw and processed) for water year 2008 with downward (upward) dz positive (negative) for visual correspondence with ΔS. (c) Schematic of seasonal analysis framework. ΔS is referenced to snow_{on} (the day $SWE > 0$). Timing of SWE_{max} (ΔS_{max}) defines the accumulation ($\text{mass}_{\uparrow}$) and ablation ($\text{mass}_{\downarrow}$) seasons. $\Delta S_{\text{snow-off}}$ is the magnitude of ΔS at snow_{off}. ΔS_{eWY} is ΔS on 30 September. SWE = snow water equivalent; SNODAS = Snow Data Assimilation System.

partitioning is determined by temperature and elevation (Lundquist et al., 2008) and ranges from 20% to 90% snow (Hunsaker et al., 2012). Precipitation that falls as snow is primarily stored in the seasonal snowpack, but also in the subsurface in areas that experience mid-winter snowmelt. Rain may also be stored in snowpack (as liquid or frozen water) but is predominantly stored in the subsurface as soil moisture or groundwater. Here, we examine the dynamics of seasonal water storage in the SN to compare aboveground storage (snow) to subsurface storage (soil moisture or groundwater), which is necessary to understand the processes that govern the partitioning of precipitation into streamflow and evapotranspiration.

Water fluxes are not measured with sufficient accuracy to reliably calculate ΔS using equation (1), either for large basins or the entire SN (Figure 1). Streamflow is reasonably well constrained by stream gage networks, although not all basins are gaged. Total precipitation is difficult to quantify, due to challenges in both remote sensing (Westrick et al., 1999; Tian & Peters-Lidard, 2010) and in situ measurement. Undercatch at sparse, high-elevation precipitation gauges increases uncertainty in interpolation-based precipitation products in topographically-complex areas like the SN (Rasmussen et al., 2012). Tower-based measurements of evapotranspiration are extremely sparse (Kerkez et al., 2012), and remote sensing-based estimates rely on proxies (e.g., Enhanced Vegetation Index) rather than direct measurement (Zhang et al., 2016). Thus, estimates of evapotranspiration are highly uncertain, even though it is likely the dominant hydrologic process during the warm season (Henn, Painter, et al., 2018).

The distribution and dynamics of seasonal SN water storage are also poorly constrained. The volume of water stored in alpine lakes and ponds is effectively unmeasured but is likely small relative to snow, soil moisture, and groundwater. Recent developments in snow remote sensing (e.g., Airborne Snow Observatory (ASO); Painter et al., 2016) have greatly improved the accuracy of snow water equivalent (SWE) estimates. By contrast, the amount and distribution of soil moisture and groundwater in the SN are largely unknown. Microwave remote sensing only measures moisture content in the upper ~5 cm of soil. In situ sensor networks are limited to a few locations (e.g., Oroza et al., 2018). High spatial variability in factors such as soil depth and hydraulic conductivity hinders extrapolation from points to the basin scale. Dividing subsurface storage between soil moisture and groundwater is challenging: typical observations and models are constrained to the top ~1 m, yet storage in variably-saturated materials below this depth but above the water

table is an important component of the water balance (Rodell & Famiglietti, 2001). Bales et al. (2011) hypothesized that substantial water mass is stored in the subsurface below 1m depth. However, this water is currently unmeasured.

GPS (Global Positioning System) vertical displacements (dz) represent a new means of quantifying changes in water mass at the mountain range scale. Permanent GPS stations monitor land surface dz resulting from instantaneous solid Earth elastic deformation associated with changes in surficial loading (Farrell, 1972; van Dam et al., 2001). GPS dz can be inverted for gridded ΔS with an effective spatial resolution determined by GPS station density. GPS dz have been used to estimate ΔS related to both seasonal (e.g., Bevis et al., 2005; Fu et al., 2012; Fu et al., 2015; Ouellette et al., 2013) and interannual processes (e.g., Argus et al., 2014; Argus et al., 2017; Borsa et al., 2014; Chew & Small, 2014). Argus et al. (2017) used monthly data to identify multiyear trends in SN ΔS, which were attributed to variations in soil moisture and/or groundwater stored deep in sediments and fractured crystalline basement. On this basis, Argus et al. (2017) suggested land surface models (LSMs) lack sufficient storage capacity to capture interannual storage.

We use daily GPS dz to quantify the seasonal dynamics of mountain range scale ΔS in the SN, considering WYs 2008–2017 individually. A framework is developed (Figure 1c) to place ΔS in the context of seasonal snow accumulation and melt and evaluate the influence of snow on seasonal mass fluctuations. We compare GPS ΔS to estimates of total precipitation. Based on these analyses, we discuss the importance of subsurface water storage in the seasonal water budget. Lastly, we consider how seasonal ΔS dynamics may change under future climate scenarios, which are expected to change precipitation partitioning—thereby impacting snowmelt (Barnhart et al., 2016) and streamflow (Berghuijs et al., 2014).

2. Methods

Procedures for inverting processed GPS dz for ΔS and assessing results are summarized below. Additional details and discussion of methodological differences between this study and Argus et al. (2017) are available in the supporting information (SI; e.g., Figure S2-1).

2.1. Seasonal ΔS From GPS dz

We used daily GPS dz time series from a total of 924 GPS stations within the spatial domain 31–50°N, 125–103°W. Since GPS dz is affected by factors other than SN hydrologic loading, we processed dz time series to isolate the signal from SN ΔS. These processing steps, which are described in detail in SI sections S1–S3, included omission of anomalously behaving stations, detrending and filtering (Figure 1b), and removal of modeled dz resulting from ΔS in large California lakes and reservoirs, Central Valley groundwater (Faunt, 2009; Xiao et al., 2017), atmospheric pressure (http://ggosatm.hg.tuwien.ac.at/loading.html), and ΔS outside the analysis domain. At nearly all stations, these adjustments to the dz time series represented <10% of the seasonal signal—confirming previous studies which show that hydrologic loading is the dominant signal on seasonal timescales (e.g., Fu et al., 2015).

For each daily time step, we inverted processed (detrended, filtered, etc.) GPS dz as in Borsa et al. (2014) to recover ΔS at every terrestrial cell of the (1/8)° study grid. We minimized the damped least squares problem

$$\|\mathbf{WGs}-\mathbf{Wd}\|_2^2 + \lambda^2\|\mathbf{Lm}\|_2^2 \tag{2}$$

where **d** is a vector of observed dz at all GPS stations for a given time step, **s** is the (unknown) equivalent water depth in all cells of the spatial domain, **W** is a weighting matrix of inverse variances in station position measurements, **L** is a smoothing matrix of spatial second differences, and λ is a minimum curvature regularization parameter, with higher values yielding smoother results (e.g., Aster et al., 2005; SI Texts S4 and S5). **G** is a design matrix containing dz responses at each station to unit loads in each grid cell, calculated with the Some Programs for Ocean Tide Loading geophysical modeling package (Agnew, 2012). Equation (2) was solved independently for each daily epoch to yield a time series of ΔS.

We corrected for smoothing-related mass leakage from the SN to its surroundings (Enzminger et al., 2018). Monthly empirical gain factors were derived from a synthetic ΔS time series using data from PRISM

(Parameter-elevation Relationships on Independent Slopes Model; Daly et al., 2008) and the NLDAS-2 (North American Land Data Assimilation System) Noah LSM (SI Text S6). This process is similar to that used to correct Gravity Recovery and Climate Experiment data (e.g., Landerer and Swenson (2012)).

Uncertainty in GPS ΔS was estimated as the spread in leakage-corrected ΔS over the SN from an ensemble of inversions. Each ensemble member consisted of an inverted ΔS time series from which data from 20 randomly selected GPS stations were withheld, and a λ between 1 and 50 was assigned (SI Text S7).

2.2. Analysis of Seasonal ΔS

We define the SN as the area within the boundaries of 13 west draining basins defined in Rosenberg et al. (2011; Figure 1a). Basin areas are based on stream gage locations near reservoirs between the SN and Central Valley. The GPS ΔS time series is the (mountain range scale) average ΔS over this area (48,147 km^2). Enzminger et al. (2018) found that GPS station density in the SN is insufficient to resolve spatial loading patterns within basins of area <10,000 km^2. We therefore limit our analysis to the mountain range scale. The challenges of treating storage and fluxes at the mountain range scale are discussed below.

We analyze GPS ΔS in the context of the seasonal water cycle (Figure 1c). For each WY, we consider ΔS relative to the start of snow accumulation ($snow_{on}$)—the day on which SN average SWE from SNODAS (Snow Data Assimilation System; NOHRSC, 2004) exceeds 1 mm. We find the magnitude of ΔS (in mm) at three times during the year: its maximum (ΔS_{max}), on the date of snow disappearance ($\Delta S_{snow\text{-}off}$), and at the end of the WY (ΔS_{eWY}). $\Delta S_{snow\text{-}off}$ represents the water available for warm season streamflow and evapotranspiration. ΔS_{eWY} represents the (positive or negative) ΔS contribution from a given WY to interannual storage. The timing of these "events" is also considered. Maximum SWE (SWE_{max}, in mm) occurs on a date which divides the snow accumulation and ablation seasons. The timing of ΔS_{max} separates analogous mass accumulation ($mass_{\uparrow}$) and loss ($mass_{\downarrow}$) seasons. $Snow_{off}$ is defined as the day average SNODAS SWE falls below 1 mm. Summer is the interval from $snow_{off}$ until the end of the WY (30 September). As SNODAS is constrained by optical remote sensing data (Carroll et al., 2001), we have confidence in the timing of $snow_{on}$ and $snow_{off}$. Analyses were repeated using a second SWE data set (Margulis et al., 2016), yielding only small differences.

We do not attempt to compare GPS ΔS to a flux-based ΔS, which would be subject to evapotranspiration measurement uncertainty. Instead, we compare GPS ΔS to accumulation season cumulative precipitation from PRISM, which should provide an upper bound on ΔS. This upper bound should not greatly exceed ΔS during the mass accumulation season—when streamflow and evapotranspiration are relatively small. We also compare GPS ΔS to LSM ΔS, or equation (1) solved with data from NLDAS-2 Noah and VIC (Variable Infiltration Capacity). Lastly, we quantify the fraction of ΔS attributable to SWE to assess the role of snowpack in ΔS.

3. Results

Over the course of each WY, SN ΔS followed a similar cycle: ΔS increased relatively steadily during fall and winter, peaked in spring, then declined over the remainder of the WY (Figure 2). On average, ΔS increased by ~1,000 mm over the $mass_{\uparrow}$ season. However, there was substantial year-to-year variability: ΔS_{max} in WY2017 exceeded 2,000 mm but was <500 mm in the drought year of WY2014 (Table 1). The duration of $mass_{\uparrow}$ and $mass_{\downarrow}$ seasons and associated rates of change similarly varied from year to year.

3.1. Comparison to Independent Data Products

3.1.1. SWE

ΔS magnitude and seasonal variations differ substantially from SWE. Averaged across years, timing of ΔS_{max} lagged SWE_{max} by 38 days (17 April vs. 10 March; Table 1). Thus, GPS ΔS indicates that water storage in the SN continues to increase after SWE begins to decline. Considered at the mountain range scale, SWE represents a small fraction of ΔS (Figures 2c and 3a). The SWE fraction of ΔS was greatest in midwinter, on average reaching ~35% in January and February. By the time of ΔS_{max}, SWE typically composed only ~20% of ΔS. When SWE from Margulis et al. (2016) was used instead of SNODAS, the fraction of ΔS from SWE increased by ~5%. The rate and duration of seasonal declines in ΔS ($mass_{\downarrow}$) and SWE (snow ablation) also differ. The SWE ablation season is roughly half the duration of the $mass_{\downarrow}$ season, and SWE ablation rates (~3 mm/day) are 60% of total mass loss rates (~5 mm/day; Figure 3b).

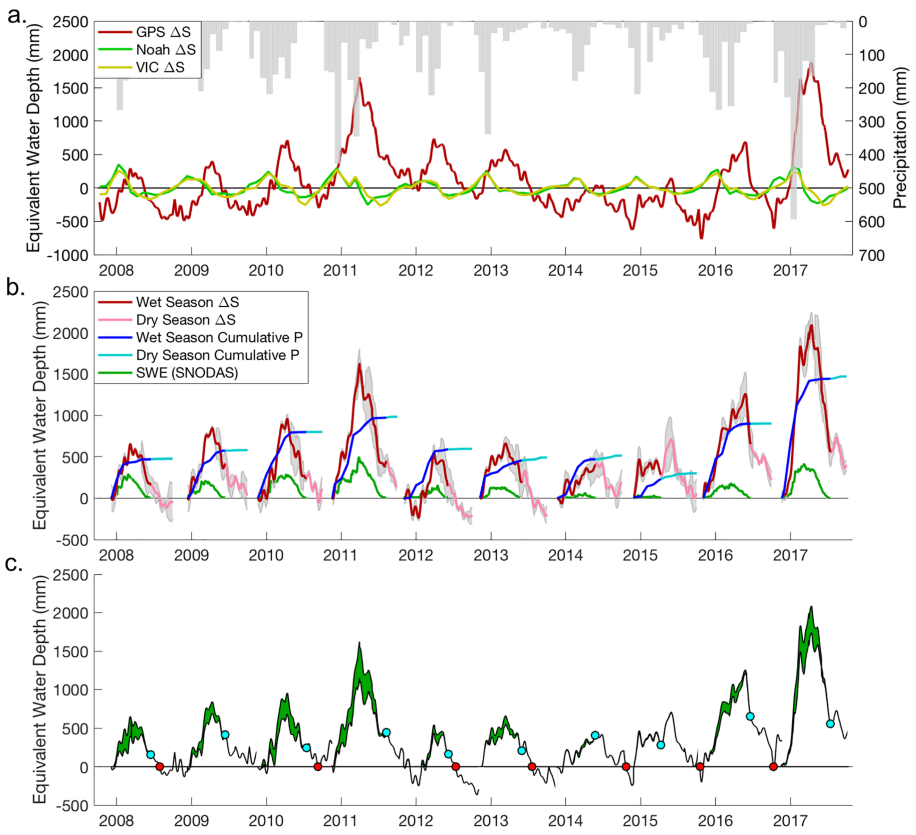

Figure 2. (a) SN ΔS from GPS dz (red) and NLDAS-2 Noah (light green) and VIC (yellow), shown with PRISM monthly precipitation (gray bars) over water years 2008–2017. (b) GPS ΔS referenced to $snow_{on}$ over the wet (red) and dry (pink) seasons, SNODAS SWE (dark green) and PRISM cumulative precipitation (blue, cyan). ΔS uncertainty is shown in gray. (c) GPS ΔS with shaded areas denoting water attributable to SNODAS SWE. $Snow_{off}$ (cyan points) and $mass_{off}$ (red points) are shown for reference. NLDAS-2 = North American Land Data Assimilation System phase 2; PRISM = Parameter-elevation Relationships on Independent Slopes Model; SWE = snow water equivalent; SNODAS = Snow Data Assimilation System; VIC = Variable Infiltration Capacity.

The observed differences between ΔS and SWE indicate that mountain range scale ΔS is not dominated by snow accumulation and subsequent melt but rather storage and loss from both the subsurface and SWE. This should not be surprising: only ~40% of the study area has persistent wet season snowpack (e.g., Figure 1a). However, the SWE we report is averaged over the entire study area. If we compare average

Table 1
Attributes of Seasonal SN ΔS

	SWE_{max}			ΔS_{max}							
Water year	$snow_{on}$	Date	Magnitude (mm)	Date	Magnitude (mm)	cum. P at ΔS_{max} (mm)	cum. $P/\Delta S_{max}$	$snow_{off}$	$\Delta S_{snow\text{-}off}$ (mm)	$mass_{off}$	ΔS_{eWY} (mm)
2008	12/6/2007	2/25/2008	290	3/7/2008	651	431	0.66	6/16/2008	159	7/28/2008	−35
2009	12/13/2008	3/7/2009	207	4/11/2009	843	487	0.58	6/13/2009	415	—	33
2010	11/20/2009	4/6/2010	284	4/13/2010	954	752	0.79	7/15/2010	242	9/8/2010	113
2011	11/19/2010	3/27/2011	492	3/31/2011	1,622	813	0.50	8/8/2011	446	—	140
2012	11/3/2011	4/15/2012	153	3/28/2012	542	548	1.01	6/5/2012	163	7/12/2012	−225
2013	11/8/2012	2/21/2013	133	3/14/2013	658	391	0.59	5/31/2013	207	7/20/2013	−198
2014	11/20/2013	4/3/2014	61	5/31/2014	423	469	1.11	5/25/2014	405	10/20/2014	198
2015	11/29/2014	12/20/2014	35	5/29/2015	708	266	0.38	4/8/2015	284	10/16/2015	57
2016	11/2/2015	3/15/2016	179	5/25/2016	1,255	895	0.71	6/19/2016	651	10/9/2016	221
2017	11/19/2016	3/7/2017	414	4/13/2017	2,087	1,418	0.68	7/14/2017	556	—	401

Note. SN = Sierra Nevada; SWE = snow water equivalent. Dates are formatted as MM/DD/YYYY.

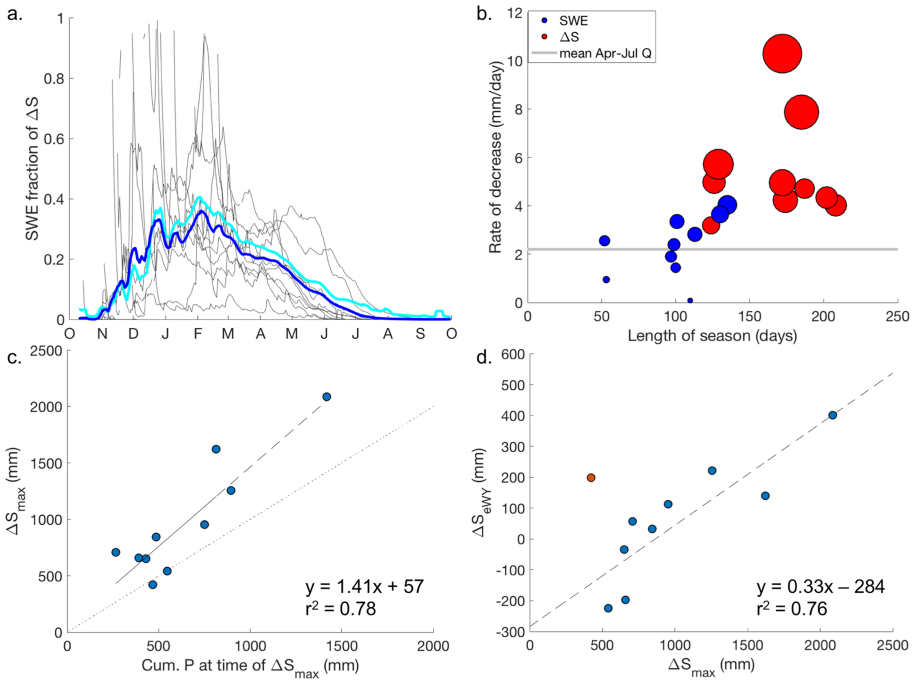

Figure 3. (a) SNODAS SWE as a fraction of ΔS. Individual water years (WYs; black) and smoothed averages (SNODAS: blue, Margulis: cyan) are shown. (b) Relationship between ablation (mass$_{\downarrow}$) season length and ablation (mass loss) rate for SWE (ΔS) across WYs. Points are sized by SWE_{max} (ΔS_{max}) in each WY. Mean 1956–2005 SN April–July streamflow (Rosenberg et al., 2011) shown for reference. (c) Relationship between cumulative precipitation at time of ΔS_{max} and ΔS_{max}. Best fit (dashed) and 1:1 (dotted) lines shown for reference. (d) Relationship between ΔS_{max} and ΔS_{eWY}. WY2014 (red) is considered an outlier, and excluded from the (dashed) best fit line. SNODAS = Snow Data Assimilation System; SWE = snow water equivalent; WY = water year; SN = Sierra Nevada.

SWE and ΔS over just the area with persistent wet season snowpack (by averaging over this region), SWE represents approximately half of ΔS at the time of ΔS_{max} and up to 75% in midwinter. Thus, even in the snowiest areas of the SN, non-snow storage is a considerable portion of ΔS. SWE ablation rates from the area with persistent wet season snowpack are of similar magnitude to mass loss rates (~6 mm/day), but ablation only occurs for approximately half the mass$_{\downarrow}$ interval.

3.1.2. Precipitation

ΔS_{max} exceeded PRISM cumulative precipitation over the mass$_{\uparrow}$ season in all but 2 years (Figure 3c and Table 1). Cumulative precipitation was on average only ~70% of ΔS_{max}, indicating that seasonal mass accumulation in the SN is significantly larger than the total precipitation mass reported by PRISM. Therefore, PRISM appears to underestimate precipitation, as precipitation should provide an upper bound on ΔS. NLDAS-2 precipitation is even lower (not shown). By contrast, PRISM cumulative precipitation and GPS ΔS_{max} are approximately equal in the area surrounding the SN (SI). Thus, the PRISM underestimation is constrained to the SN, confirming previously reported low biases in interpolation-based precipitation products over mountainous areas (e.g., Immerzeel et al. (2015); Henn, Clark, et al. (2018)). GPS ΔS indicates that this underestimation is more pronounced in wetter years (Figure 3c).

3.1.3. ΔS From LSMs

There is little agreement between GPS ΔS and Noah and VIC ΔS. Seasonal GPS ΔS fluctuations exceeded those from LSMs by nearly an order of magnitude. Additionally, the timing of seasonal variations does not match: LSM ΔS generally peaked at the beginning of the GPS mass$_{\uparrow}$ season and declined during the interval in which the rate of GPS ΔS increase was greatest (Figure 2a).

3.2. Water Storage After Snow Melt: $\Delta S_{snow\text{-}off}$

$\Delta S_{snow\text{-}off}$ was positive in every WY in our analysis (Figure 2b). $\Delta S_{snow\text{-}off}$ varied from 159 to 651 mm, or ~25–50% of ΔS_{max}, depending on the WY (Table 1). A modest correlation ($r^2 = 0.46$, not shown) between ΔS_{max}

and $\Delta S_{snow\text{-}off}$ suggests that additional water added to the mountains during the wet season yields additional storage at $snow_{off}$.

3.3. Interannual Storage: ΔS_{eWY}

Year-to-year changes in SN water storage are indicated by ΔS_{eWY}: when ΔS_{eWY} is positive (negative), water from the preceding WY is retained within (lost from) the mountains. We find that multiyear changes in SN water storage are small in comparison to the large year-to-year variations in precipitation and ΔS. However, by detrending over the study interval, we remove secular signals which may be partly due to multiyear ΔS trends. This methodological difference between this study and Argus et al. (2017) is not expected to affect the results of the seasonal analysis. Despite detrending, the pattern of interannual storage agrees with Argus et al. (2017): Consistent ΔS_{eWY} in sequential years leads to multiyear trends in water storage, as seen in the general increase in ΔS from 2008 to 2011 and the decrease from 2011 to 2016 (Figure 2a).

Using our seasonal framework (Figure 1c), we compare ΔS_{eWY} to ΔS_{max} and precipitation. A strong positive correlation exists ($r^2 = 0.76$) between ΔS_{eWY} and ΔS_{max} or cumulative precipitation for 9 of the 10 WYs examined (Figure 3d). In the 3 years with the greatest ΔS_{max} and precipitation, ΔS_{eWY} averaged ~250 mm. By contrast, ΔS_{eWY} was below or near zero in dry years. Thus, water is added to the SN during wet years and lost during dry years. WY2014 does not follow this pattern: ΔS_{eWY} was ~200 mm even though ΔS_{max} and precipitation were below average. Noise in the GPS record or unusual late summer precipitation are possible explanations for this outlier.

4. Discussion

If the magnitudes we obtained for GPS ΔS_{max} are correct, our results imply that PRISM precipitation is too low by 25% or more in the SN. Leakage in the GPS inversion displaces water from the SN to the surrounding area, which we corrected via linear rescaling. A leakage "overcorrection" might move too much water back into the mountains, leaving SN ΔS too high. While leakage-corrected ΔS within the SN exceeds cumulative precipitation, leakage-corrected ΔS outside the SN is approximately equal to cumulative precipitation (SI). This agreement suggests that we have not overcorrected for SN mass leakage. Lack of gauge undercatch correction—which is known to bias precipitation estimates by up to 20% (Rasmussen et al., 2012; Serreze et al., 1999)—and relatively low gauge density at high elevations may explain the low bias in PRISM precipitation reported here and elsewhere (e.g., Henn, Clark, et al. (2018)).

GPS ΔS suggests that SN water storage is not dominated by SWE but by subsurface storage of rainfall and snowmelt that is primarily released via evapotranspiration. Lower elevation portions of SN basins are subject to more precipitation (Hunsaker et al., 2012) and more intermittent intervals of SWE accumulation and melt (Rice et al., 2011) compared to high elevations. It is therefore reasonable that ΔS exceeds independent estimates of SWE. Our estimate that SWE comprises ~30% of ΔS during the wet season agrees with recent independent estimates of snow as a fraction of total precipitation (Li et al., 2017). However, we caution that these results are contingent on the leakage correction used to return mass to the SN. With no leakage correction—which increases ΔS by up to a factor of two in some years (SI Figure S6-3)—we would report a SWE fraction of ΔS >50%. Leakage correction based on a different ΔS model would also affect the results, albeit to a much smaller degree (Enzminger et al., 2018).

While GPS ΔS reveals substantial seasonal nonsnow storage, it cannot discern the vertical distribution of stored water. Lakes and ponds cover <1% of the SN, and we have accounted for the effects of large reservoirs and lakes. Therefore, seasonal mass fluctuations likely occur predominantly in the subsurface. Given the lack of information concerning depth, extent, and hydraulic properties of soils and regolith in the SN, it is not possible to determine whether water is stored as soil moisture or groundwater or at what depths.

We hypothesize that the bulk of subsurface storage must be shallow enough to be accessible to evapotranspiration. Rosenberg et al. (2011) showed that streamflow removes ~2 mm/day during the $mass_{\downarrow}$ season (April–July; Figure 3b and SI). As GPS ΔS suggests that mass is lost at rates ≥5 mm/day during the $mass_{\downarrow}$ season, >60% of mass must be lost as evapotranspiration. Evapotranspiration appears to be larger in wet years, based on annual differences between ΔS_{max} and ΔS_{eWY}. The majority of subsurface water must therefore be accessible to plant root uptake and/or soil evaporation and thus stored no more than several meters deep. Bales et al. (2011) hypothesized that approximately one third of annual SN evapotranspiration must

come from below 1-m depth, which is essentially unmonitored. On interannual timescales, positive increments in ΔS likely result from infiltration of a relatively small fraction (~10–20%) of water into deep soils and bedrock fractures, as proposed by Argus et al. (2017). This study illustrates the need for improved monitoring of both soil and groundwater, as there is no in situ monitoring that allows for testing these hypotheses.

Argus et al. (2017) concluded that NLDAS-2 Noah is an incomplete representation of hydrologic processes on interannual timescales; our results extend this conclusion to seasonal timescales and NLDAS-2 VIC. Subsurface storage in many LSMs is explicitly limited to several 100-mm equivalent water depth of soil moisture (e.g., Liang et al., 1994). We find that nonsnow ΔS substantially exceeds this amount in every WY (Figure 2c). Thus, there is no way for these LSMs to represent the seasonal variability in SN subsurface storage measured by GPS.

Due to GPS network density constraints, GPS ΔS provides limited information on spatial loading patterns within individual basins. Thus, future research should pursue synthesis of GPS dz with other sources of hydrologic data and models (e.g., SWE from ASO). GPS dz may be useful in constraining ΔS in LSMs, particularly given the need for improved subsurface representation and the likelihood that precipitation inputs are underestimated.

Projected future changes in the regional climate have significant implications for the SN water balance. While the magnitude of average annual precipitation is expected to remain unchanged, less precipitation will fall as snow under future conditions (IPCC, 2014). Currently, ~30% of precipitation falling as snow generates ~74% of regional annual streamflow (Li et al., 2017). Reductions in annual snowfall are likely to reduce total streamflow (e.g., Berghuijs et al. (2014); Barnhart et al. (2016)). Our results suggest that the SN's shallow subsurface is capable of storing vast amounts of water. Thus, seasonal ΔS may not change under future climate conditions, but storage may shift from the snowpack to the subsurface. This shift could increase evapotranspiration and lower streamflow, thereby reducing downstream water availability.

Acknowledgments
This work was funded by NSF Grants EAR-1521474 and EAR-1521127. PRISM data were acquired via ftp from the PRISM climate group (http://www.prism.oregonstate.edu/mtd/). NLDAS-2 data were acquired via the Giovanni system, maintained by the NASA GES DISC. SNODAS data were acquired via ftp from the National Snow and Ice Data Center. Snow reanalysis data from Margulis et al. (2016) were downloaded directly from the https://margulis-group.github.io/data/ website. Groundwater data from Xiao et al. (2017) were downloaded directly from the https://ucla.app.box.com/v/data-grl-ca-groundwaterloss website. California Central Valley Hydrologic Model data were acquired from the https://ca.water.usgs.gov/projects/central-valley/central-valley-hydrologic-model.html website. ΔS data from Argus et al. (2017) were acquired for comparison from the ftp://garner.ucsd.edu/pub/projects/eseses.2019/ website. We thank Dr. Jeff Freymueller and Dr. Donald Argus for improving the paper with their helpful reviews. We thank Dr. Debi Kilb for providing California surface water body shapefiles. Inverted ΔS and leakage correction grids generated in this study can be accessed via the University of Colorado Boulder Institutional Repository (scholar.colorado.edu).

References

Agnew, D. C. (2012). SPOTL: Some programs for ocean-tide loading, 44.
Argus, D. F., Fu, Y., & Landerer, F. W. (2014). Seasonal variation in total water storage in California inferred from GPS observations of vertical land motion. *Geophysical Research Letters*, *41*, 1971–1980. https://doi.org/10.1002/2014GL059570
Argus, D. F., Landerer, F. W., Wiese, D. N., Martens, H. R., Fu, Y., Famiglietti, J. S., et al. (2017). Sustained water loss in California's mountain ranges during severe drought from 2012 to 2015 inferred from GPS. *Journal of Geophysical Research: Solid Earth*, *122*, 10,559–10,585. https://doi.org/10.1002/2017JB014424
Aster, R. C., Borchers, B., & Thurber, C. (2005). *Parameter estimation and inverse problems*. Burlington, MA: Elsevier Academic Press.
Bales, R. C., Hopmans, J. W., O'Geen, A. T., Meadows, M., Hartsough, P. C., Kirchner, P., et al. (2011). Soil moisture response to snowmelt and rainfall in a Sierra Nevada mixed-conifer forest. *Vadose Zone Journal*. https://doi.org/10.2136/vzj2011.0001
Barnhart, T. B., Molotch, N. P., Livneh, B., Harpold, A. A., Knowles, J. F., & Schneider, D. (2016). Snowmelt rate dictates streamflow. *Geophysical Research Letters*, *43*, 8006–8016. https://doi.org/10.1002/2016GL069690
Berghuijs, W. R., Woods, R. A., & Hrachowitz, M. (2014). A precipitation shift from snow towards rain leads to a decrease in streamflow. *Nature Climate Change*. https://doi.org/10.1038/nclimate2246
Bevis, M., Alsdorf, D., Kendrick, E., Fortes, L. P., Forsberg, B., Smalley, R., & Becker, J. (2005). Seasonal fluctuations in the mass of the Amazon River system and Earth's elastic response. *Geophysical Research Letters*, *32*, L16308. https://doi.org/10.1029/2005GL023491
Borsa, A. A., Agnew, D. C., & Cayan, D. R. (2014). Ongoing drought-induced uplift in the western United States. *Science*, *345*(6204), 1587–1590. https://doi.org/10.1126/science.1260279
Carroll, T., Cline, D., Fall, G., Nilsson, A., Li, L., & Rost, A. (2001). NOHRSC operations and the simulation of snow cover properties for the coterminous U.S., *69th Annu. Meet. West. Snow Conf.*, 1–14.
Chew, C. C., & Small, E. E. (2014). Terrestrial water storage response to the 2012 drought estimated from GPS vertical position anomalies. *Geophysical Research Letters*, *41*, 6145–6151. https://doi.org/10.1002/2014GL061206
Daly, C., Halbleib, M., Smith, J. I., Gibson, W. P., Doggett, M. K., Taylor, G. H., et al. (2008). Physiographically sensitive mapping of climatological temperature and precipitation across the conterminous United States. *International Journal of Climatology*. https://doi.org/10.1002/joc.1688
Doesken, N. J., & Judson, A. (1996). *The snow booklet: A guide to the science, climatology, and measurement of snow in the United States*, (2nd ed.). Fort Collins: Colorado Climate Center.
Enzminger, T. L., Small, E. E., & Borsa, A. A. (2018). Accuracy of snow water equivalent estimated from GPS vertical displacements: A synthetic loading case study for western U.S. mountains. *Water Resources Research*, *54*, 581–599. https://doi.org/10.1002/2017WR021521
Farrell, W. E. (1972). Deformation of the Earth by surface loads. *Reviews of Geophysics*, *10*(3), 761–797. https://doi.org/10.1029/RG010i003p00761
Faunt, C. C., Ed. (2009). Groundwater availability of the Central Valley Aquifer, California: U.S. *Geological Survey Professional paper 1766*.
Fu, Y., Argus, D. F., & Landerer, F. W. (2015). GPS as an independent measurement to estimate terrestrial water storage variations in Washington and Oregon. *Journal of Geophysical Research: Solid Earth*, *120*, 552–566. https://doi.org/10.1002/2014JB011415
Fu, Y., Freymueller, J. T., & Jensen, T. (2012). Seasonal hydrological loading in southern Alaska observed by GPS and GRACE. *Geophysical Research Letters*, *39*, L15310. https://doi.org/10.1029/2012GL052453

Henn, B., Clark, M. P., Kavetski, D., Newman, A. J., Hughes, M., McGurk, B., & Lundquist, J. D. (2018). Spatiotemporal patterns of precipitation inferred from streamflow observations across the Sierra Nevada mountain range. *Journal of Hydrology*. https://doi.org/10.1016/j.jhydrol.2016.08.009

Henn, B., Painter, T. H., Bormann, K. J., McGurk, B., Flint, A. L., Flint, L. E., et al. (2018). High-elevation evapotranspiration estimates during drought: Using streamflow and NASA airborne snow observatory SWE observations to close the upper Tuolumne river basin water balance. *Water Resources Research*, *54*, 746–766. https://doi.org/10.1002/2017WR020473

Hunsaker, C. T., Whitaker, T. W., & Bales, R. C. (2012). Snowmelt runoff and water yield along elevation and temperature gradients in California's Southern Sierra Nevada. *Journal of the American Water Resources Association*. https://doi.org/10.1111/j.1752-1688.2012.00641.x

Immerzeel, W. W., Wanders, N., Lutz, A. F., Shea, J. M., & Bierkens, M. F. P. (2015). Reconciling high-altitude precipitation in the upper Indus basin with glacier mass balances and runoff. *Hydrology and Earth System Sciences*. https://doi.org/10.5194/hess-19-4673-2015

IPCC (2014). In Core Writing Team, R. K. Pachauri, & L. A. Meyer (Eds.), *Climate Change 2014: Synthesis Report. Contribution of Working Groups I, II and III to the Fifth Assessment Report of the Intergovernmental Panel on Climate Change*, (p. 151). Geneva, Switzerland: IPCC.

Kerkez, B., Glaser, S. D., Bales, R. C., & Meadows, M. W. (2012). Design and performance of a wireless sensor network for catchment-scale snow and soil moisture measurements. *Water Resources Research*, *48*, W09515. https://doi.org/10.1029/2011WR011214

Landerer, F. W., & Swenson, S. C. (2012). Accuracy of scaled GRACE terrestrial water storage estimates. *Water Resources Research*, *48*, W04531. https://doi.org/10.1029/2011WR011453

Li, D., Wrzesien, M. L., Durand, M., Adam, J., & Lettenmaier, D. P. (2017). How much runoff originates as snow in the western United States, and how will that change in the future? *Geophysical Research Letters*, *44*, 6163–6172. https://doi.org/10.1002/2017GL073551

Liang, X., Lettenmaier, D. P., Wood, E. F., & Burges, S. J. (1994). A simple hydrologically based model of land surface water and energy fluxes for general circulation models. *Journal of Geophysical Research*, *99*(D7), 14415. https://doi.org/10.1029/94JD00483

Lundquist, J. D., Neiman, P. J., Martner, B., White, A. B., Gottas, D. J., & Ralph, F. M. (2008). Rain versus snow in the Sierra Nevada, California: Comparing Doppler profiling radar and surface observations of melting level. *Journal of Hydrometeorology*, *9*(2), 194–211. https://doi.org/10.1175/2007JHM853.1

Margulis, S. A., Cortés, G., Girotto, M., & Durand, M. (2016). A Landsat-Era Sierra Nevada snow reanalysis (1985–2015). *Journal of Hydrometeorology*, *17*(4), 1203–1221. https://doi.org/10.1175/jhm-d-15-0177.1

National Operational Hydrologic Remote Sensing Center (2004). *Snow Data Assimilation System (SNODAS) data products at NSIDC*. Boulder, CO: National Snow and Ice Data Center. Digital media.

Oroza, C. A., Bales, R. C., Stacy, E. M., Zheng, Z., & Glaser, S. D. (2018). Long-term variability of soil moisture in the southern Sierra: Measurement and prediction. *Vadose Zone Journal*, *17*(1). https://doi.org/10.2136/vzj2017.10.0178

Ouellette, K. J., De Linage, C., & Famiglietti, J. S. (2013). Estimating snow water equivalent from GPS vertical site-position observations in the western United States. *Water Resources Research*, *49*, 2508–2518. https://doi.org/10.1002/wrcr.20173

Painter, T. H., Berisford, D. F., Boardman, J. W., Bormann, K. J., Deems, J. S., Gehrke, F., et al. (2016). The airborne snow observatory: Fusion of scanning LIDAR, imaging spectrometer, and physically-based modeling for mapping snow water equivalent and snow albedo. *Remote Sensing of Environment*, *184*, 139–152. https://doi.org/10.1016/j.rse.2016.06.018

Rasmussen, R., Baker, B., Kochendorfer, J., Meyers, T., Landolt, S., Fischer, A. P., et al. (2012). How well are we measuring snow: The NOAA/FAA/NCAR winter precipitation test bed. *Bulletin of the American Meteorological Society*, *93*(6), 811–829. https://doi.org/10.1175/bams-d-11-00052.1

Rice, R., Bales, R. C., Painter, T. H., & Dozier, J. (2011). Snow water equivalent along elevation gradients in the Merced and Tuolumne River basins of the Sierra Nevada. *Water Resources Research*, *47*, W08515. https://doi.org/10.1029/2010WR009278

Rodell, M., & Famiglietti, J. S. (2001). An analysis of terrestrial water storage variations in Illinois with implications for the Gravity Recovery and Climate Experiment (GRACE). *Water Resources Research*, *37*(5), 1327–1339. https://doi.org/10.1029/2000WR900306

Rosenberg, E. A., Wood, A. W., & Steinemann, A. C. (2011). Statistical applications of physically based hydrologic models to seasonal streamflow forecasts. *Water Resources Research*, *47*, W00H14. https://doi.org/10.1029/2010WR010101

Serreze, M. C., Clark, M. P., Armstrong, R. L., McGinnis, D. A., & Pulwarty, R. S. (1999). Characteristics of the western United States snowpack from snowpack telemetry (SNOTEL) data. *Water Resources Research*, *35*(7), 2145–2160. https://doi.org/10.1029/1999WR900090

Tian, Y., & Peters-Lidard, C. D. (2010). A global map of uncertainties in satellite-based precipitation measurements. *Geophysical Research Letters*, *37*, L24407. https://doi.org/10.1029/2010GL046008

van Dam, T., Wahr, J., Milly, P. C. D., Shmakin, A. B., Blewitt, G., Lavallée, D., & Larson, K. M. (2001). Crustal displacements due to continental water loading. *Geophysical Research Letters*, *28*(4), 651–654. https://doi.org/10.1029/2000GL012120

Westrick, K. J., Mass, C. F., & Colle, B. A. (1999). The limitations of the WSR-88D radar network for quantitative precipitation measurement over the coastal western United States. *Bulletin of the American Meteorological Society*, *80*(11), 2289–2298. https://doi.org/10.1175/1520-0477(1999)080<2289:TLOTWR>2.0.CO;2

Xiao, M., Koppa, A., Mekonnen, Z., Pagán, B. R., Zhan, S., Cao, Q., et al. (2017). How much groundwater did California's Central Valley lose during the 2012–2016 drought? *Geophysical Research Letters*, *44*, 4872–4879. https://doi.org/10.1002/2017GL073333

Zhang, K., Kimball, J. S., & Running, S. W. (2016). A review of remote sensing based actual evapotranspiration estimation. *Wiley Interdisciplinary Reviews Water*, *3*(6), 834–853. https://doi.org/10.1002/wat2.1168